2. Monoene Kinetics*

The kinetics of hydrogenation and isomerization of edible oils are poorly understood and general rate equations are not available. Because of the relevance to industrial applications, usually polyunsaturated oils have been investigated, which has resulted in apparent rate equations containing many fit parameters. In this chapter, the intrinsic kinetics of monoene hydrogenation are studied to serve as a key component both in the elaborate reaction mechanism of polyene hydrogenation and in the study of intraparticle diffusion limitation. The construction of the reaction framework and subsequent possible rate-determining elementary reaction steps is a main objective of this chapter, followed by the selection of the most relevant rate equations from statistical analysis of the experimental results.

* Published as "Intrinsic kinetics of 9-monoeneic fatty acid methyl ester hydrogenation over nickel-based catalysts"; by Jonker, G. H.; Veldsink, J. W.; Beenackers, A. A. C. M. *Ind. Eng. Chem. Res.*, **1997**, *36*, 1567–1579.

2.1. Introduction

This chapter considers the kinetics of hydrogenation of monoenes. These are simpler to understand than those of polyenes because fewer side products are made, which enables a more thorough investigation of the elementary reaction steps (e.g., Hashimoto et al., 1971; Heertje and Boerma, 1971; Bern et al, 1975b; Cordova and Harriott, 1975; Susu et al., 1978; Tsuto et al., 1978; Gut et al., 1979; Coenen, 1986). Also in monoene hydrogenation, undesired products are formed, due to migration and *cis–trans* isomerization of double bonds. The *cis–trans* isomerization was explained from the formation of a half-hydrogenated surface intermediate (Allen and Kiess, 1955; Hashimoto et al., 1971; Gut et al., 1979; Albright, 1985; Grau et al., 1988) and its easy rotation at the surface (Dutton et al., 1968; Heertje et al., 1974; Van der Plank and Van Oosten, 1975), whereas migration occurs via the π-allyl intermediate, the latter of which is mainly present at low hydrogen pressure (Heertje et al., 1974; Van der Plank and Van Oosten, 1975). In this study, we focus on the formation of the half-hydrogenated intermediate only. It is the key component of the well-known Horiuti–Polanyi mechanism (Horiuti and Polanyi, 1934). The different reactions that can occur in the hydrogenation of monoenes are shown in Figure 2.1. The two possible monoenes *cis* (O, oleic) and *trans* (E, elaidic) can both adsorb on the catalyst (k_a and k_d); this is denoted by a bar above their symbols. The adsorbed species can react reversibly with a single hydrogen atom to form an intermediate SH (k_f and k_b). This intermediate can revert to the original reactant, it may isomerize or it may react further with hydrogen to the saturated S (stearic), which will then desorb. The second hydrogen insertion (k_h) is practically irreversible; all other reactions are reversible.

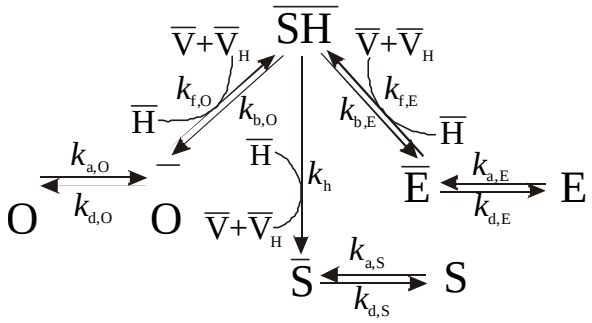

Figure 2.1. Hydrogenation scheme of monounsaturated FAME according to the Horiuti–Polanyi mechanism.

Monoene hydrogenation kinetics are often assumed to be first order in the concentration of unsaturated bonds (Coenen, 1960; Cousins and Feuge, 1960; Nielsen et al., 1960; Stefanovic and Albright, 1969; Marangozis et al., 1977; Drozdowski and Zajac, 1980; Stenberg and Schöön, 1985; Colen et al., 1988), but orders varying between 0 and 1 have also been observed (Vandenheuvel, 1956; Hashimoto et al., 1971; Bern et al., 1975b; Susu et al., 1978; Lidefelt et al., 1983). The application of

Langmuir–Hinshelwood–Hougen–Watson (LHHW) kinetics is a more fundamental approach, which consists of a rate-determining reaction step (usually a surface reaction step), combined with Langmuir adsorption of reactants and products (Weller, 1992). The LHHW-based kinetic rate equations of Hashimoto et al. (1971), Gut et al. (1979), and Grau et al. (1986), for monoene hydrogenation are based on apparent kinetics, but as we will show below, our rate equations appear to cover their findings. However, a thorough investigation of the rate-determining steps in the monoene edible oil hydrogenation is not available from open literature.

Apart from the LHHW approach, the steady-state approximation can be applied over the most reactive compound (Froment and Hosten, 1981). Although the steady-state method is also of interest, we have selected the LHHW approach because it provided us with a logical way of deriving rate equations in relation to the reaction mechanism and gives a good tool to extend the models to polyunsaturated compounds. Moreover, nickel-catalyzed fat hydrogenation can be classified as structure-insensitive heterogeneous catalysis (Coenen, 1986) for which Weller (1992) recommends the LHHW or "classical kinetics", because of its proven applicability. Recent results in surface science techniques at Ni(111) surfaces show non-Langmuirian adsorption of hydrogen (Johnson et al., 1992), which, however, cannot (yet) be extended to discuss the application of LHHW techniques under industrial circumstances.

In kinetic studies, methyl esters of fatty acids (FAME) are preferred relative to triacylgycerides (TAG), because the larger TAGs may suffer from diffusion limitation in the pores (Feuge, 1955; Coenen, 1976; Tsuto et al., 1978; Coenen, 1986; Colen et al., 1988; Grau et al., 1988). TAG and FAME hydrogenation kinetics are believed to be the same, because the reaction kinetics appear to be influenced by the direct surroundings of the double bond in the fatty acid chain only (Van der Plank, 1972a,b). Further, FAMEs can be analyzed directly on isomer formation and degree of saturation by high-temperature gas chromatography.

We studied the rate-determining reaction steps in the hydrogenation of monoene FAME with the aim to obtain mechanistically realistic, LHHW-based, intrinsic rate equations. We consider *cis–trans* isomerization only and follow the Horiuti–Polanyi mechanism. Only at lower hydrogen pressures double bonds appeared to migrate along the carbon chain, merely one position only. The characteristics of the double bonds from the 8, 9, or 10 position can be assumed to be similar, because the surroundings are always comparable. Besides, at most conditions, the migration products are only minor, compared to *cis–trans* isomerization products. We systematically derived

different sets of rate equations, each with a unique set of rate-determining steps. The rate equations were subsequently evaluated for a wide range of experimental data obtained with an industrial nickel-based catalyst (Pricat 9910). Bartlett's test was used to compare the significance of the set of rate equations (Dumez et al., 1977; Graaf et al., 1988a,b). All possible combinations were evaluated, including sets of rate equations which are unlikely from a physical point of view, to test thoroughly our statistical analysis.

2.2. Theory

2.2.1. Hydrogenation Mechanism. The reactions consist of isomerization between O and E, and saturation of the double bonds to form S, see Figure 2.1. Table 2.1 shows the rate equations of the reaction steps of the Horiuti–Polanyi mechanism (HP), and the corresponding equilibrium constants in terms of liquid concentrations (denoted by C) and surface fractions ($\sum q_i = 1$, i = O,E,S,SH,V; $q_H + q_{V_H} = 1$).

A distinction can be made between adsorption steps (A1, B1, C1 and D) and surface reaction steps (A2, B2, C2), see Table 2.1 (and Figure 2.1). The adsorption of O and E at the surface (A1 and B1) is followed by (the first) insertion of hydrogen to form the half-hydrogenated intermediate (A2 and B2). A second hydrogen insertion (C2) yields a completely saturated product, which gives, after desorption (C1), S (stearate, methyl octadecanoate). The adsorption of hydrogen may be controlled either by the rate of adsorption on the surface (associative adsorption (D-a)) or by the subsequent dissociation in hydrogen atoms (dissociative adsorption (D-d)).

Apart from the second hydrogen insertion, all reaction steps are reversible with characteristic equilibrium constants. The second hydrogen insertion can be regarded as an irreversible reaction, because dehydrogenation occurs above 670 K only (Feuge, 1955). The equilibrium constant for the O–E reaction is defined as:

$$K_{iso} = \frac{C_E}{C_O} = \frac{K_O K_{I,O}}{K_E K_{I,E}} \qquad (2.1)$$

The reported values vary between 2 and 4 (Feuge et al., 1951; Litchfield et al., 1963; Gut et al., 1979; Grau et al., 1986). The equilibrium ratio is independent of hydrogen pressure (see eq 2.1) and depends weakly on temperature, $\Delta H_{iso} = -4$ kJ/mol (Rogers et al., 1977). In our kinetic analysis each reaction step is allowed to either control the overall conversion rate or to proceed close to equilibrium. The adsorption of the double bonds of O and E on the supported nickel surface (A1 and B1) is usually

assumed to be at equilibrium (Vandenheuvel, 1956; Van der Plank, 1972a,b; Zwicky and Gut, 1978; Gut et al., 1979), though nonequilibrium adsorption has also been incorporated to fit experimental data (Tsuto et al., 1978; Grau et al., 1986; Münzing et al., 1986). Van der Plank and Van Oosten (1975) have concluded from migration of the double bonds of the monoene FAME molecule that the first hydrogen insertion should be rate determining. In deriving our rate equations, we have allowed for any possible combination of rate-determining steps.

Table 2.1: Reaction Steps according to Horiuti–Polanyi Mechanism

code	reaction eq	R_{ES}/m_c	equilibrium constant
A1	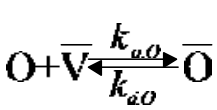	$k_{a,O}C_O q_V - k_{d,O} q_O$	$K_O = \frac{k_{a,O}}{k_{d,O}} = \frac{q_O}{C_O q_V}$
B1	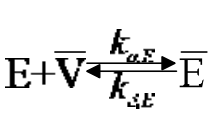	$k_{a,E}C_E q_V - k_{d,E} q_E$	$K_E = \frac{k_{a,E}}{k_{d,E}} = \frac{q_E}{C_E q_V}$
C1	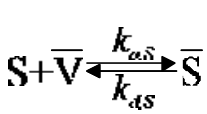	$k_{a,S}C_S q_V - k_{d,S} q_S$	$K_S = \frac{k_{a,S}}{k_{d,S}} = \frac{q_S}{C_S q_V}$
D-a	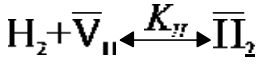		$K_H = \frac{q_H}{P_{H_2} q_{V_H}}$
D-d	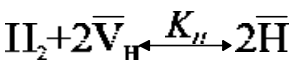		$K_H = \frac{q_H^2}{P_{H_2} q_{V_H}^2}$
A2	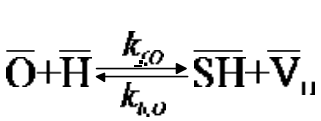	$k_{f,O} q_O q_H - k_{b,O} q_{SH} q_{V_H}$	$K_{I,O} = \frac{k_{f,O}}{k_{b,O}} = \frac{q_{SH} q_{V_H}}{q_O q_H}$
B2	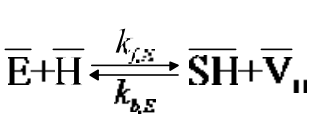	$k_{f,E} q_E q_H - k_{b,E} q_{SH} q_{V_H}$	$K_{I,E} = \frac{k_{f,E}}{k_{b,E}} = \frac{q_{SH} q_{V_H}}{q_E q_H}$
C2	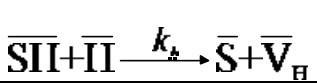	$k_h q_{SH} q_H$	

2.2.2. Rate equations. To derive rate expressions, we divided the overall, integral reaction network (Figure 2.1) into three distinct reactions as shown in Table 2.2 (Graaf

et al., 1988a,b). From these reactions of Table 2.2, only two are independent, which restricts the choice of rate determining steps for the hydrogenation reactions.

Table 2.2. Reaction Paths

reaction path	overall equation	elementary reaction steps
hydrogenation of oleate	$O + 2\overline{H} = S + 2\overline{V}_H$	A1-A2-C2-C1
hydrogenation of elaidate	$E + 2\overline{H} = S + 2\overline{V}_H$	B1-B2-C2-C1
isomerisation reaction	$O = E$	A1-A2-B2-B1

For each model, the rate equations for the observed reaction rates of O and E are composed of the contributions of two reaction paths

$$R_O = R_{O,h} + R_{iso} \tag{2.2}$$

$$R_E = R_{E,h} - R_{iso} \tag{2.3}$$

The $R_{O,h}$ is the reaction or conversion rate of O in the hydrogenation path of O to S and $R_{E,h}$ of the path of E to S. Although the isomerization path shares reaction steps with the hydrogenation paths (see Figure 2.1), the reaction rate of the isomerization R_{iso} is taken to be independent of the hydrogenation of O and E.

Further basic model assumptions are as follows:

1. The intermediates are in a pseudo steady state, which implies equal reaction rates of elementary steps along one reaction path (Froment and Hosten, 1981; Graaf 1988; Graaf et al., 1988a,b).

2. The catalyst sites are uniform and homogeneously distributed (Marangozis et al., 1977; Gut et al., 1979; Grau et al., 1986).

3. Two types of adsorption sites are used to account for independent adsorption of hydrogen (V_H) and FAME (V) (Marangozis et al., 1977; Gut et al., 1979; Grau et al., 1986; Rodrigo et al., 1992). In the gas phase, with FAME concentrations of around 5% of hydrogen, hydrogen and FAME reportedly compete for the same active nickel sites (Lidefelt et al., 1983; Magnusson, 1987a,b), but in the liquid phase the FAME is present in large excess and, owing to the large differences in molecular sizes, the small hydrogen most likely adsorbs on sites between the large FAME molecules only (Marangozis et al., 1977).

4. O, E, and S are assumed to compete for the same surface sites, with a negligible amount of vacant sites (Gut et al., 1979).

5. The adsorption constant of O is considered to be equal to that of E, $K_O=K_E\equiv K_M$ (Gut et al., 1979; Grau et al., 1986). K_M stands for the adsorption constant of the monoene.

6. The surface occupation of the half-hydrogenated intermediate is negligible compared to that of bulk components (Zwicky and Gut, 1978; Graaf et al., 1988a,b). In deriving LHHW-type rate equations, surface intermediates are usually neglected in the (competitive) adsorption of bulk components for vacant surface sites (Weller, 1992). It should be remarked that assumption 6 is only made after the rate equations are derived, to reduce the number of parameters in the denominator of the Langmuir-type equations.

7. Hydrogen adsorption is at equilibrium, relative to the hydrogen concentration in the liquid close to the catalyst surface; see Table 2.1, D-a and D-d for definitions.

The mass balances of the mole fractions of FAME and hydrogen at the surface thus read:

$$q_O + q_E + q_S = 1 \tag{2.4}$$

$$q_H + q_{V_H} = 1 \tag{2.5}$$

A kinetic model consists of two rate-determining steps, one for each independent reaction. The other steps are considered to be at equilibrium. Because each reaction path involves four elementary steps, there are 16 possibilities. However, the hydrogenation reactions O and E share identical reaction steps (C1 and C2), which decreases the number of combinations from 16 to (2 x 2 + 2 =) 6 combinations or models. These models are identified as A1B1, A1B2, A2B1, A2B2, C1C1 and C2C2; the coding refers to the rate-determining reaction steps.

The overall rate equations are derived as follows. For model A1B1, the elementary rate equations of the reaction paths are

$$R_{O,h} = -m_c k_{a,O}^{O,h}(C_O q_V - K_O^{-1} q_O) \text{ (A1)} \tag{2.6}$$

$$R_{E,h} = -m_c k_{a,E}^{E,h}(C_E q_V - K_E^{-1} q_E) \text{ (B1)} \tag{2.7}$$

$$R_{iso} = -m_c k_{a,O}^{iso}(C_O q_V - K_O^{-1} q_O) = m_c k_{a,E}^{iso}(C_E q_V - K_E^{-1} q_E) \quad \text{(A1/B1)} \tag{2.8}$$

Table 2.3: Rate Equations

model	R_O/m_c	R_E/m_c
A1B1	$\dfrac{-(k_{a,O}^{O,h}+\bar{k}_1^{iso}K_{iso})C_O+\bar{k}_1^{iso}C_E}{K_O^{\#}C_O+K_E^{\#}C_E+K_SC_S}$	$\dfrac{-(k_{a,E}^{E,h}+\bar{k}_1^{iso})C_E+\bar{k}_1^{iso}K_{iso}C_O}{K_O^{\#}C_O+K_E^{\#}C_E+K_SC_S}$
A1B2	$\dfrac{-(k_{a,O}^{O,h}K_M^{-1}(1+K_{E,O}^{iso}K_{iso}\theta_H)+k_{f,E}^{iso}K_{iso}\theta_H)C_O+k_{f,E}^{iso}\theta_HC_E}{\psi_OC_O+(1+K_{E,O}^{iso}(\psi_O+K_{iso})\theta_H)C_E+\bar{K}_S(1+K_{E,O}^{iso}K_{iso}\theta_H)C_S}$	$\dfrac{-(k_{f,E}^{E,h}(1+K_{E,O}^{iso}K_{iso}\theta_H)+k_{f,E}^{iso})\theta_HC_E+k_{f,E}^{iso}K_{iso}\theta_HC_O}{\psi_OC_O+(1+K_{E,O}^{iso}(\psi_O+K_{iso})\theta_H)C_E+\bar{K}_S(1+K_{E,O}^{iso}K_{iso}\theta_H)C_S}$
A2B1	$\dfrac{-(k_{f,O}^{O,h}(1+K_{O,E}^{iso}K_{iso}^{-1}\theta_H)+k_{f,O}^{iso})\theta_HC_O+k_{f,O}^{iso}\theta_HC_E}{\psi_EC_E+(1+K_{O,E}^{iso}(\psi_E+K_{iso}^{-1})\theta_H)C_O+\bar{K}_S(1+K_{O,E}^{iso}K_{iso}\theta_H)C_S}$	$\dfrac{-(k_{a,E}^{E,h}K_M^{-1}(1+K_{O,E}^{iso}K_{iso}^{-1}\theta_H)+k_{f,O}^{iso}K_{iso}^{-1}\theta_H)C_E+k_{f,O}^{iso}\theta_HC_O}{\psi_EC_E+(1+K_{O,E}^{iso}(\psi_E+K_{iso}^{-1})\theta_H)C_O+\bar{K}_S(1+K_{O,E}^{iso}K_{iso}\theta_H)C_S}$
A2B2	$\dfrac{-(k_{f,O}^{O,h}+\bar{k}_2^{iso}K_{iso})\theta_HC_O+\bar{k}_2^{iso}\theta_HC_E}{C_O+C_E+\bar{K}_SC_S}$	$\dfrac{-(k_{f,E}^{E,h}+\bar{k}_2^{iso})\theta_HC_E+\bar{k}_2^{iso}K_{iso}\theta_HC_O}{C_O+C_E+\bar{K}_SC_S}$
C1C1	$\to\infty$	$\to\infty$
C2C2	$-\dfrac{(k_h^{O,h}+k_h^{E,h})K_{I,O}C_O\ \theta_H^2}{C_O+C_E+\bar{K}_SC_S\quad\theta_{V_H}}$	$-\dfrac{(k_h^{O,h}+k_h^{E,h})K_{I,O}K_{iso}^{-1}C_E\ \theta_H^2}{C_O+C_E+\bar{K}_SC_S\quad\theta_{V_H}}$

A1B1: $\bar{k}_1^{iso}=\dfrac{k_{a,O}^{iso}k_{a,E}^{iso}}{k_{a,O}^{iso}+K_{iso}k_{a,E}^{iso}}$ $\quad K_O^{\#}=\dfrac{2\psi_O\bar{k}_1^{iso}K_{iso}K_M}{k_{a,E}^{iso}}$ $\quad K_E^{\#}=\dfrac{2\psi_E\bar{k}_1^{iso}K_{iso}K_M}{k_{a,O}^{iso}}$ $\quad$ A2B2: $\bar{k}_2^{iso}=\dfrac{k_{f,O}^{iso}k_{f,E}^{iso}}{k_{f,O}^{iso}+K_{iso}k_{f,E}^{iso}}$

$K_{E,O}^{iso}=\dfrac{K_Mk_{f,E}^{iso}}{k_{a,O}^{iso}}$ $\quad K_{O,E}^{iso}=\dfrac{K_Mk_{f,O}^{iso}}{k_{a,E}^{iso}}$ $\quad \bar{K}_S=\dfrac{K_S}{K_M}$ $\quad \psi_O=\dfrac{k_{a,O}^{iso}}{k_{a,O}^{iso}+k_{a,O}^{O,h}}$ $\quad \psi_E=\dfrac{k_{a,E}^{iso}}{k_{a,E}^{iso}+k_{a,E}^{E,h}}$ $\quad \theta_H$: eq 2.9/2.10

The hydrogenation paths ($R_{O,h}$ and $R_{E,h}$) and the isomerization path (R_{iso}) are

independent paths, each with characteristic rate constants, which are in the case of the rate constant $k_{a,O}$ (eqs 2.6–2.8) denoted by $k_{a,O}^{O,h}$, $k_{a,O}^{E,h}$, and $k_{a,O}^{iso}$, respectively. The equilibrium constants for elementary reactions A2, B2, C1 and C2 (the latter goes to infinity) can be used to solve the unknown surface fractions from eqs 2.6–2.8. In the final expressions for the rate equations, the equilibrium constant for the isomerization reaction is substituted (eq 2.1).

For dissociative equilibrium hydrogen adsorption, the hydrogen fraction at the surface is

$$q_H = \frac{\sqrt{K_H P_{H_2}}}{1+\sqrt{K_H P_{H_2}}} \tag{2.9}$$

and for associative equilibrium adsorption

$$q_H = \frac{K_H P_{H_2}}{1+K_H P_{H_2}} \tag{2.10}$$

If hydrogen adsorption plays a role in the model rate equations, the applied hydrogen equilibrium adsorption is denoted by ass (associative) or diss (dissociative), e.g., A2B2-ass and A2B2-diss. Table 2.3 summarizes the overall rate equations for O and E for each of the six models.

The model C1C1 predicts an unrealistically high reaction rate, because the irreversible reaction of the half hydrogenated intermediate to S is now 'close to equilibrium', implying an infinite reaction rate. Therefore, this model not further considered.

The independent variables (O, E, and S concentrations and hydrogen pressure) of the remaining five models are preceded by groups of parameters of elementary steps. Only the value of the group of parameters can be obtained. Therefore, the groups of parameters are replaced by lumped parameters, for each model denoted by $k_1 \ldots k_6$. Table 2.4 gives the rate equations which were used to fit the experimental results, by adjusting the lumped parameters. Comparison of Tables 2.3 and Table 2.4 gives the group of parameters of elementary reaction steps which are represented by the lumped parameters.

The temperature dependency of the lumped parameters is assumed to obey an Arrhenius relation:

Table 2.4: Rate Equations of Table 2.3 in Terms of Lumped Parameters[a]

model	R_O/m_c	R_E/m_c
A1B1	$\frac{-(k_1+k_2K_{iso})C_O+k_2C_E}{C_O+k_5C_E+k_4C_S}$	$\frac{-(k_3+k_2)C_E+k_2K_{iso}C_O}{C_O+k_5C_E+k_4C_S}$
A1B2	$\frac{-(k_1(1+k_6K_{iso}q_H)+k_2K_{iso}q_H)C_O+k_2q_HC_E}{C_O+(1+k_6(1+K_{iso})q_H)C_E+k_4(1+k_6K_{iso}q_H)C_S}$	$\frac{-(k_3(1+k_6K_{iso}q_H)+k_2)q_HC_E+k_2K_{iso}q_HC_O}{C_O+(1+k_6(1+K_{iso})q_H)C_E+k_4(1+k_6K_{iso}q_H)C_S}$
A2B1	$\frac{-(k_1(1+k_6K_{iso}^{-1}q_H)+k_2)q_HC_O+k_2K_{iso}^{-1}q_HC_E}{C_E+(1+k_6(1+K_{iso}^{-1})q_H)C_O+k_4(1+k_6K_{iso}^{-1}q_H)C_S}$	$\frac{-(k_3(1+k_6K_{iso}^{-1}q_H)+k_2K_{iso}^{-1}q_H)C_E+k_2q_HC_O}{C_E+(1+k_6(1+K_{iso}^{-1})q_H)C_O+k_4(1+k_6K_{iso}^{-1}q_H)C_S}$
A2B2	$\frac{-(k_1+k_2K_{iso})q_HC_O+k_2q_HC_E}{C_O+C_E+k_4C_S}$	$\frac{-(k_3+k_2)q_HC_E+k_2K_{iso}q_HC_O}{C_O+C_E+k_4C_S}$
C2C2	$\frac{-k_1q_H^2q_{V_H}^{-1}C_O}{C_O+C_E+k_4C_S}$	$\frac{-k_1K_{iso}^{-1}q_H^2q_{V_H}^{-1}C_E}{C_O+C_E+k_4C_S}$

[a] diss: $q_H=k_5P_{H_2}/(1+k_5P_{H_2})$; ass: $q_H=\sqrt{k_5P_{H_2}}/(1+\sqrt{k_5P_{H_2}})$; $q_{V_H}=1-q_H$

$$k_i(T)=k_{i,\mathrm{ref}}\exp\left(-\frac{E_{a,i}}{R_{gas}T_{ref}}\left(\frac{T_{ref}-T}{T}\right)\right)\qquad i=1,\ldots,6 \tag{2.11}$$

Two literature models can be used to compare model A2B2 with associative hydrogen adsorption: for the simplified hydrogenation scheme of Figure 2.2, Hashimoto et al. (1971) and Gut et al. (1979) (and also Zwicky and Gut, 1978) derived on the basis of the LHHW approach rate equations similar to model A2B2, with k_3 equal to k_1. Hashimoto et al. (1971) assumed dissociative and Gut et al. (1979) associative hydrogen adsorption. The equations were tested on hydrogenations with TAGs over a nickel catalyst (Hashimoto et al., 1971; Gut et al., 1979). Grau et al. (1986) derived rate equations on the basis of the Horiuti–Polanyi mechanism, which were evaluated using monoene hydrogenation over nickel catalysts, but due to their calculation method, only the *cis–trans* isomerization equilibrium constant is available to compare to our data.

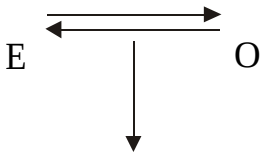

Figure 2.2. Generalized hydrogenation scheme of Gut et al. (1979).

2.2.3. Transport phenomena. Because hydrogenation of edible oils or FAMEs is a three-phase process, several transport limitations may occur and should be avoided in kinetic studies (Westerterp et al., 1987). In hydrogenation, the mass-transfer limitations for hydrogen and FAME have been frequently recognised as the rate-determining processes (Marangozis et al., 1977). Therefore, the volumetric mass-transfer coefficient, $k_l a$, which depends on the reactor configuration, has been measured separately in the experimental setup used in this study. Catalyst loads were adjusted until the observed conversion rate was below 2% of the maximum hydrogen gas/liquid absorption rate.

To eliminate effects of pore hindrance, FAMEs were used instead of TAGs, but also in the case of FAMEs, a careful check on intra-particle mass transport effects is needed if knowledge of the rate expression is absent (Van der Plank, 1972b). The influence of intraparticle diffusion limitation of hydrogen and FAME was checked by calculating the Weisz–Prater number (Froment and Bischoff, 1979) for the initial hydrogenation rate (Bern et al., 1975a; Zwicky and Gut, 1978; Grau et al., 1986) which is given by:

$$\Phi_i = \frac{(-R_i) m_{\mathrm{Ni}} r_{\mathrm{c}} d_{\mathrm{p}}^2}{36 m_{\mathrm{c}} D_{\mathrm{e},i} C_i} \qquad i = \mathrm{O}, \mathrm{E}, \mathrm{H}_2 \tag{2.12}$$

The criterion for the absence of mass-transfer limitation for unknown kinetics is $\Phi_i < 0.03$–0.7 (Westerterp et al., 1987). When the rate equation is known, the intraparticle concentration profiles can be calculated from:

$$D_{\mathrm{e},i} \frac{\mathrm{d}}{\mathrm{d}r_{\mathrm{p}}} \left[r_{\mathrm{p}}^2 \frac{\mathrm{d}C_i}{\mathrm{d}r_{\mathrm{p}}} \right] = \frac{r_{\mathrm{c}} m_{\mathrm{Ni}}}{m_{\mathrm{c}}} R_i r_{\mathrm{p}}^2 \qquad i = \mathrm{O}, \mathrm{E}, \mathrm{H}_2 \tag{2.13}$$

The hydrogen uptake rate equals the sum of the oleate and elaidate reaction rate:

$$R_{\mathrm{H}_2} = -(R_{\mathrm{O}} + R_{\mathrm{E}}) \tag{2.14}$$

The effectiveness factor for component i follows from the calculated flux to the particle and the maximum possible reaction rate related to the bulk concentrations C_{b} (Westerterp et al., 1987):

$$m_i = \frac{J_i a_c}{R_i(C_{b,i})} \qquad i = \mathrm{O, E, H_2} \qquad (2.15)$$

In absence of diffusion limitations, the reaction rates for a dead end batch reactor are:

$$\frac{dC_{b,i}}{dt} = R_i \qquad i = \mathrm{O, E, H_2} \qquad (2.16)$$

2.3. Experimental Section

The hydrogenation of FAME was carried out in a 600 mL agitated, dead-end autoclave, equipped with an automatic sampler and a custom-made oven for in situ catalyst reduction, see Figure 2.3. The additional oven contains a cup in which the catalyst particles were placed before the reaction starts, to regenerate the catalyst at P_{H_2} = 0.5 MPa and T = 473 K for 2 h, followed by deodorization under vacuum for 0.5 h. The autoclave was well stirred (25 rps, with baffles), and the reactor temperature was controlled within 1 K. When the desired reaction pressure and temperature were reached, the reaction was started by putting the cup in the reaction mixture. Induction periods, which may be caused by impurities (Drozdowski and Zajac, 1980), or insufficient preactivation of the catalyst (Coenen, 1960; Grau et al., 1987a) were not observed during the experimental runs.

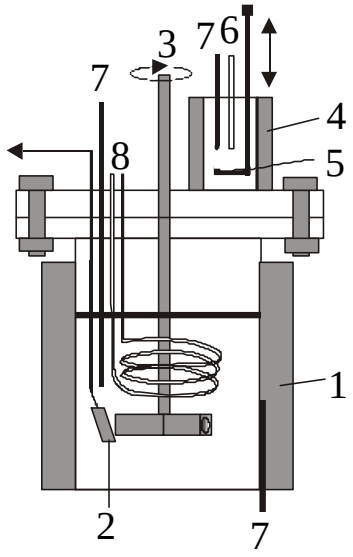

Figure 2.3. Experimental setup: 1, reactor oven; 2, filter and sample tube; 3, self-inducing stirrer; 4, oven for catalyst activation; 5, cup; 6, hydrogen supply tube; 7, temperature control; 8, cooling coil.

Hydrogen was supplied from a storage vessel and its consumption could be measured by monitoring the decrease of the pressure in this vessel with time. Liquid

samples were stored in a 16-loop valve. Afterwards, their liquid composition (O, E, S) was determined by gas–liquid chromatography (Hewlett Packard 5890, supplied with a Chrompack CP-sil 88 column). The standard deviation of the fractions O, E, and S was found to be 20% of the measured value at low mole fractions (0.0–0.1), 10% at moderate fractions (0.1–0.3), and 5% at high fractions (0.3–1.0).

We performed two types of experiments:

a. Constant Hydrogen Pressure. In these experiments, the autoclave was operated at constant hydrogen pressure by continuously supplying hydrogen from a storage vessel. During the course of the reaction, up to 15 samples were automatically taken from the reaction mixture and analyzed afterwards. Hence, the experimental data consisted of mass fraction distributions of O, E, and S (Figure 2.4) together with the hydrogen consumption as a function of time. Experiments were carried out for $333 \leq T \leq 413$ K and $0.02 \leq P_{H_2} \leq 0.50$ MPa. At partial hydrogen pressures below 0.2 MPa, nitrogen was used to balance the total reactor pressure at 0.2 MPa, which was necessary to collect samples.

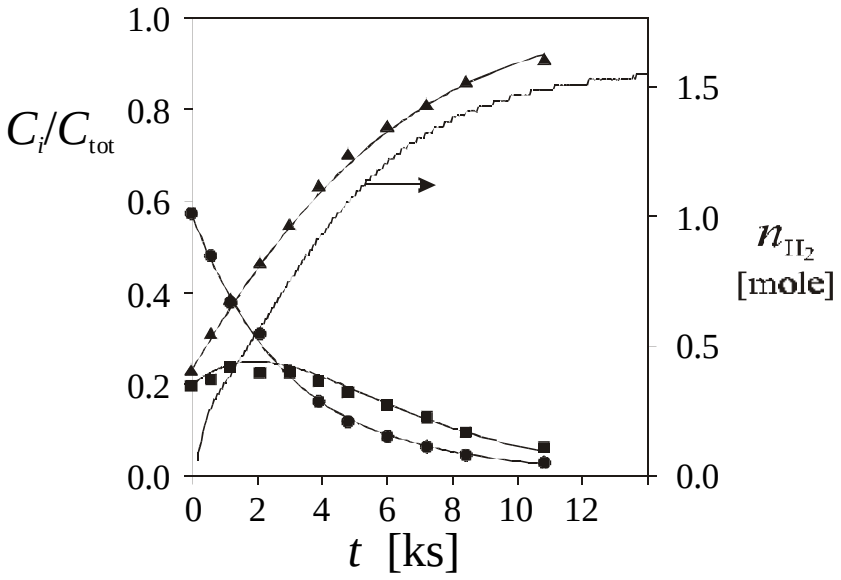

Figure 2.4. Liquid-phase composition and hydrogen uptake in a constant hydrogen pressure experiment, as a function of reaction time for a typical oleate hydrogenation run. The hydrogen uptake is equal to the amount of produced stearate. Conditions: 413 K, 0.5 MPa, 0.120 kg_{Ni}/m_l^3, l, O; n, E; s, S.

b. Varying Hydrogen Pressure. Here, hydrogen was consumed from the head space of the autoclave without additional supply from the storage bottle. During such

an experiment, the hydrogen pressure dropped from about 0.40 MPa to 0.01 MPa. (Figure 2.5), while the conversion of FAME remained below 7%. As a result, the liquid-phase composition remained approximately constant. These experiments were

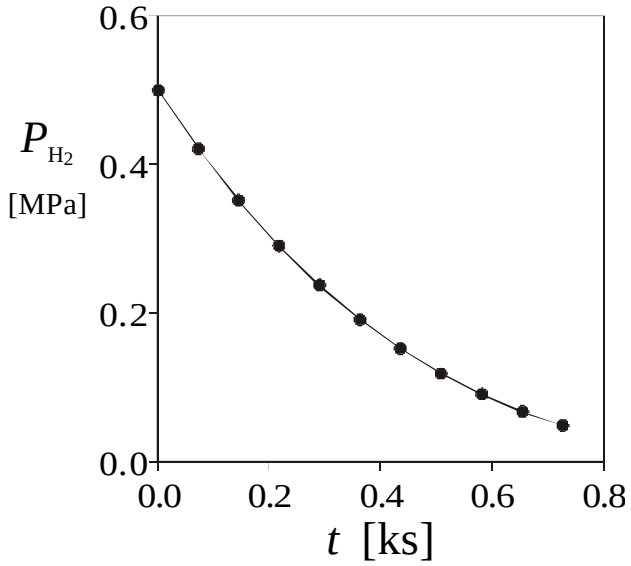

Figure 2.5. Reactor pressure during a typical experiment with varying hydrogen pressure. Conditions: 353 K, 0.177 kg_{Ni}/m_l^3.

carried out at $353 \leq T \leq 413$ K.

The reactor contents were nickel catalyst, hydrogen and various mixtures of FAME. The catalyst was Pricat 9910 (Unichema), d_p= 8.4 *m*m, present in flakes of hardened fat. Hydrogen was supplied by Hoekloos, with a purity of >99.999%. FAME mixtures of various initial compositions were used, see Table 2.5.

To test the rate equations properly, we used both HPE (high percentage of E) and HPO (high percentage of O) mixtures. The HPE (60% E) was made by partial and selective hydrogenation of methyl esters of sunflower (initially 70% methyl linoleate, 2-fold unsaturated 9-*cis*-12-*trans*-octadecenoate) at 443 K and 0.08 MPa. HPO (68% O) was obtained from Unichema, Gouda, The Netherlands. In the latter experiments, reaction rates relative to the overall hydrogenation rate could be used only, because the relatively high sulfur contents (21 ppm) partly inhibited the active sites (Feuge, 1955; Nielsen et al., 1960; Stefanovic and Albright, 1969; Drozdowski and Zajac, 1980; Stenberg and Schöön, 1985; Edvarsson and Irandoust, 1993). Therefore, oleate-rich mixtures were also prepared from sulfur-free (less than 0.1 ppm) methyl esters of

Table 2.5: Initial Compositions of FAME Mixtures

code	%O	%E	%S
HPO	68	22	10
MPO	45	20	35
HPE	60	25	15

sunflower, at 353 K and 0.50 MPa, yielding maximally 45% O (medium percentage of O, MPO). As expected, the MPO and HPO mixtures (Nielsen et al., 1960; Edvarsson and Irandoust, 1993) gave the same results in the conversion domain, where the isomerization rate relative to the hydrogenation rate is considered only. Although of most value for model evaluation, purified unsaturated FAMEs were not used because these are very hard to obtain in sufficiently large quantities and chemically derived O and E contain different amounts of minor compounds which influence the hydrogenation.

The experimental series consist of HPO, HPE, and MPO experiments with both constant and variable hydrogen pressure. The complete conversion range was analyzed to derive rate equations which are applicable to a large range of reactant concentrations. Table 2.6 summarizes the experimental series.

Table 2.6. Experiments: Pressure (MPa) and Temperature (K) Combinations [a]

mix	exp	T = 333	T = 353	T = 373	T = 393	T = 413
HPO	CP		0.25/0.50	0.25/0.50	0.25/0.50	0.25/0.50
HPE	CP		0.02/0.08		0.50	
MPO	CP	0.50	0.25/0.50	0.50	0.08–0.50	
	VP		0.40–0.0	0.40–0.0	0.40–0.0	0.40–0.0

[a] HPO, HPE = high percentage of oleate, elaidate, respectively; MPO = medium percentage of oleate; CP = constant hydrogen pressure experiment; VP = variable hydrogen pressure experiment.

2.4 Results and Discussion

The volumetric gas–liquid mass-transfer coefficient, $k_l a$, was separately measured at an excess of catalyst load, 3.0 wt % (Stenberg and Schöön, 1985; Beenackers and Van Swaaij, 1993). The result was $k_l a$=1.8 s^{-1}, independent of catalyst load. Values of $k_l a$ up to 1 s^{-1} for a comparable reactor setup with similar fluids were found by Dietrich et al. (1992). We calculated that the influence of the gas-side mass-transfer resistance in the nitrogen–hydrogen experiments is negligible. For all experiments, the ratio between gas–liquid mass transfer and total reaction rate was below 2%.

Intraparticle diffusion limitations for hydrogen and FAME were estimated from the Weisz–Prater number (eq 2.12) and the initial hydrogenation rates. The hydrogen concentration in the liquid was calculated using m_{H_2} = 0.1 m_g^3/m_l^3 at 393 K (extrapolated from Ganguli and Van den Berg, 1978; see also Ganguli, 1975). Intraparticle diffusion coefficients for the Pricat 9910 were taken as $D_{e,H_2} = 2 \times 10^{-9}$ m^2/s (Andersson et al., 1974; Ganguli, 1975; Ganguli and Van den Berg, 1978; Tsuto et al., 1978; Stenberg and Schöön, 1985) and $D_{e,O} = D_{e,E} = 2 \times 10^{-11}$ m^2/s (Andersson et al., 1974; Tsuto et al., 1978; Colen et al, 1988). Other values are: d_p = 8.4 *m*m and r_c = 264 kg_{Ni}/m_c^3. In our experiments, the numerical value of the Weisz–Prater modules always remained below 0.1. Therefore, we have strong evidence that no intraparticle diffusion occurred in our experiments.

In each model evaluation, K_{iso} = 3.5 (T = 393 K). This value was obtained from independent isomerization experiments of monoene FAME with selenium (Litchfield et al., 1963). Other reported values of K_{iso} were determined from kinetic data (Feuge et al., 1960; Stefanovic et al., 1969; Grau et al., 1986) and may contain ratios of kinetic rate constants, see section 2.4.3. The temperature dependency is ΔH_{iso} = –4 kJ/mol (Rogers et al., 1977).

The five models with associative or dissociative hydrogen adsorption were subsequently evaluated in both the conversion and the time domain. To reduce the number of parameters, first an optimization was performed on the ratios of rate constants in the conversion domain, followed by a second optimization in the time domain. Model selection was performed both by Bartlett's test and physical interpretation of the model fits.

2.4.1. Conversion Domain. For parameter optimization in the conversion domain, the rate equations were rewritten as a function of the double-bond conversion or the degree of hydrogenation. Advantages of this method are as follows: (1) reduction of the number of parameters, because the parameters are now obtained as a ratio to the total hydrogenation rate constant, denoted by k_2^c (=k_2/k_1) and k_3^c (=k_3/k_1). For example, the rate equations of model A1B1 in the conversion domain read

$$R_O^c = \frac{R_O}{R_S} = \frac{-(1 + k_2^c K_{iso}) C_O + k_2^c C_E}{C_O + k_3^c C_E} \tag{2.17}$$

$$R_E^c = \frac{R_E}{R_S} = \frac{-(k_3^c + k_2^c)C_E + k_2^c K_{iso} C_O}{C_O + k_3^c C_E} \qquad (2.18)$$

(2) Reduction of the number of models, because A1B1 and A2B2 become identical in the conversion domain. (3) Elimination of effects of contaminations (sulfur) on activity (Edvarsson and Irandoust, 1993). The optimization of the parameters started with the estimation of the rate constants at the reference temperature (393 K), followed by the estimation of the activation energies in the whole temperature range.

The compound parameters k_5 and k_6 in models A1B2 and A2B1 (Table 2.4) were found to be highly correlated (>95%) to parameters k_2^c and k_3^c, which asks for a decrease of parameters in these models. For k_5 it was found:

hydrogen equilibrium ($333 \le T \le 413$ K, $0.02 \le P_{H_2} \le 0.50$ MPa):

associative $k_5 P_{H_2} << 1$ (eq 2.10)

dissociative $Ö(k_5 P_{H_2}) << 1$ (eq 2.9) (2.19)

For monoene FAME hydrogenations, Marangozis et al. (1977), Gut et al. (1979) and Stenberg and Schöön (1985) also found first-order behavior in hydrogen.

Table 2.7. Parameter k_6 in models A1B2 and A2B1

case	assumption for A1B2	assumption for A2B1	parameters optimized		
1	none	none	k_2^c	k_3^c	k_6
2	$k_6 K_{iso} q_H >> 1$	$k_6 (K_{iso})^{-1} q_H >> 1$	k_2^c/k_6	k_3^c	
3	$k_6 K_{iso} q_H << 1$	$k_6 (K_{iso})^{-1} q_H << 1$	k_2^c	k_3^c	

Table 2.8. Total Variances (S_h^2 /10^4) for Models A1B2 and A2B1 [a]

model	q_H	case 1	case 2	case 3
A1B2	ass	3.00	3.67	5.98
	diss	1.43	1.55	3.72
A2B1	ass	3.96	3.92	18.0
	diss	2.94	2.92	10.2

[a] Cases 1, 2, 3: see Table 2.7. q_H hydrogen adsorption equilibrium, which can be associative (ass) or dissociative (diss). Total variance defined in Appendix eq 2.A3

Therefore, in further optimizations, we took a linear (associative adsorption) or a square root (dissociative) hydrogen adsorption equilibrium.

A further reduction of the parameters in models A1B2 and A2B1 was possible from an examination of the role of parameter k_6. Three cases can be considered, see Table 2.7. For case 1 three parameters have to be optimised (k_2^c, k_3^c, and k_6), whereas in asymptotic cases 2 and 3 the number of parameters decreases from three to two.

For all three cases, Table 2.8 gives the total variances for models A1B2 and A2B1. In case 1, the parameter values are meaningless (due to a high correlation, k_2^c and k_6 adopt extremely large values), but it is possible to calculate the total variances. For k_6=0 (case 3, $k_6 K_{iso} q_H << 1$), the total variances considerably increase. However, case 2 proves to be equally accurate as case 1, so the following assumption can be applied:

$$\begin{aligned} k_6 K_{iso} q_H &>> 1 \text{ (model A1B2)} \\ k_6 K_{iso}^{-1} q_H &>> 1 \text{ (model A2B1)} \end{aligned} \qquad (2.20)$$

Table 2.9. Total Variances in Conversion Domain [a]

model	q_H	C, 393 $S_h^2 \times 10^4$	C, 393 rank	C, all $S_h^2 \times 10^4$	C, all rank
A1B1		2.62	2	2.63	2
A1B2	ass	3.67	4	5.73	5
A1B2	diss	1.55	1	2.46	1
A2B1	diss	3.96	5	3.32	3
A2B1	ass	2.92	3	4.54	4
A2B2	ass	2.62	2	2.63	2
A2B2	diss	2.62	2	2.63	2
C2C2		173	6		

[a] C,393 = reference temperature (393 K), df = 36; C,all = whole temperature range, df = 74 (both conversion domain). q_H = hydrogen adsorption equilibrium, associative (ass) or dissociative (diss). rank = ranking in accuracy.

Table 2.10: Bartlett's test for conversion domain [a]

c^2	$H = 6$	$H = 5$	$H = 4$	$H = 3$	$H = 2$
c_t^2	11.1	9.49	7.81	5.99	3.84
c_c^2: C,393	369	<u>8.88</u>	<u>6.58</u>	<u>3.81</u>	<u>2.42</u>
c_c^2: C,all		19.5	<u>8.77</u>	<u>1.86</u>	<u>0.08</u>

[a] C,393, C,all, see Table 2.9. c_c^2: critical c^2, Bartlett's test (eq 2.A2). c_t^2: tabulated c^2 (Fisher, 1970).

This way, the number of parameters in models A1B2 and A2B1 is reduced from 4 (k_2^c, k_3^c, k_5 and k_6) to 2: k_2^c/k_6 and k_3^c. Optimization in the conversion domain gave a first selection of models. Table 2.9 shows the total variances per model for all optimisations in the conversion domain and their ranking. The total variances serve as an input for Bartlett's test (Table 2.10). The *H* denotes the number of collated models, in succeeding order: $H = 6$ are the best six of the models, $H = 5$ the best five, etc.

Bartlett's test (Appendix: eq 2.A2) compares c_c^2 to the tabulated value c^2_t (Fisher, 1970) for H - 1 degrees of freedom. The underlined values represent the corresponding best *H* models, which do not differ significantly from the best model. The selected best models are A1B2-diss, A2B1-diss, A1B2-ass, A2B1-ass, and A1B1, the latter which also represents A2B2-ass and A2B2-diss because the rate equations are similar in the conversion domain.

According to Bartlett's test for the first optimization step in the conversion domain, at constant temperature, model C2C2 is significantly more inaccurate than the other models (Table 2.9 and 2.10). Model C2C2 is unrealistic, because, it assumes that all reactions in the isomerization path are at equilibrium and implies that the isomerization rate should be instantaneous, which is not found experimentally (see Figure 2.4). The other models are statistically indistinguishable, and therefore in the first optimization step, only model C2C2 is removed from the list of models.

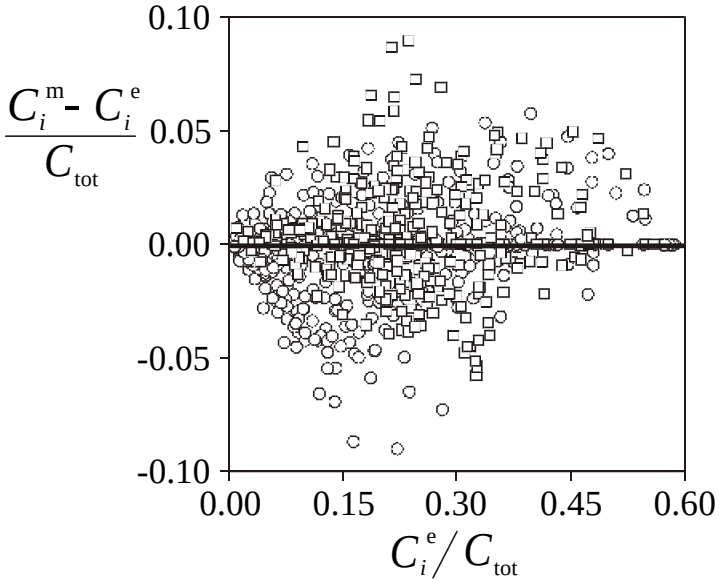

Figure 2.6. Residuals between the model and experiment for a fit in the conversion domain (whole temperature range) for model A1B2 with associative hydrogen adsorption equilibrium; ○, oleate; □, elaidate.

The second step was optimization of activation energies in the conversion domain (using the whole temperature range). Now A1B2-diss, A1B1 (and therefore also A2B2-ass and A2B2-diss), A2B1-ass, and A2B1-diss remained statistically indistinguishable. The c^2 of model A1B2-ass proved to be significantly larger compared to the other models (Table 2.9), which was confirmed by Bartlett's test (Table 2.10). Bartlett's test is visualized in Figures 2.6 and 2.7, which show the large deviations between experimental and predicted mole fractions of model A1B2-ass (Figure 2.6) compared to A1B2-diss (Figure 2.7). So, model A1B2-ass was also removed from the list of models.

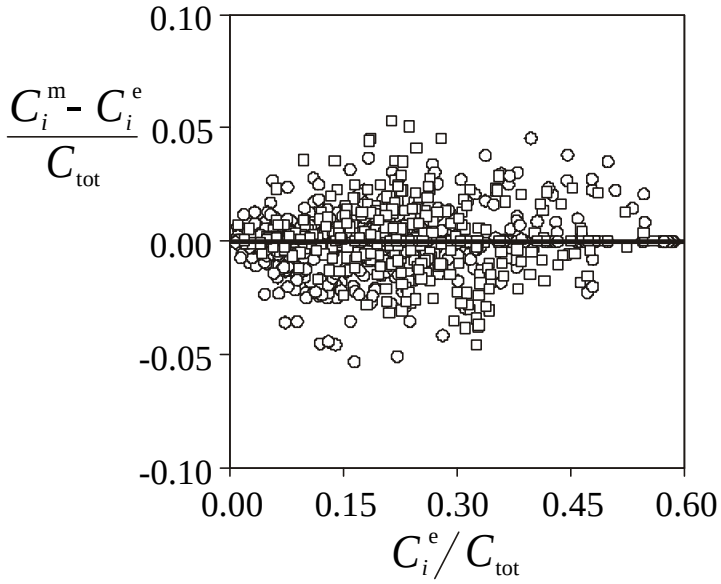

Figure 2.7. Residuals between the model and experiment for a fit in the conversion domain (whole temperature range) for model A1B2 with dissociative hydrogen adsorption equilibrium: ○, oleate; □, elaidate.

2.4.2. Time domain. In the time domain, the remaining models A1B2-diss, A1B1, A2B1-ass, A2B1-diss, A2B2-ass, and A2B2-diss were tested by estimation of the k_1 and the adsorption parameters using the optimised values of k_2^{c} and k_3^{c}, found in the conversion domain.

After an estimation of the value of the lumped rate constant, k_1, at the reference temperature, the three parameters $E_{\mathrm{a}1}$, $k_{1,\mathrm{ref}}$, and k_4 were simultaneously optimized over the whole temperature range. The parameter k_4, a ratio of adsorption constants, appeared to be independent of T.

Bartlett's test (Table 2.12), based on the S_h^2 of Table 2.11, restricted the possible best models to A2B2-ass and A2B1-ass. In model A1B1, the hydrogen function is absent, which is unrealistic in the time domain, and consequently model A1B1 was rejected by Bartlett's test ($H = 6$, $c_c^2 = 33.4$). Also rejected were the two models with a dissociative hydrogen function: A2B2-diss and A2B1-diss.

Table 2.11: Total Variances in Time Domain [a]

model	q_H	$S_h^2 \times 10^4$	rank
A1B1		103	6
A1B2	diss	51.3	5
A2B1	ass	16.6	2
A2B1	diss	37.3	3
A2B2	ass	12.1	1
A2B2	diss	45.0	4

[a] df = 23. q_H: hydrogen adsorption equilibrium, associative or dissociative. rank: ranking in accuracy

Table 2.12. Bartlett's Test for Time Domain [a]

c^2	$H = 6$	$H = 5$	$H = 4$	$H = 3$	$H = 2$
c_t^2	11.1	9.49	7.81	5.99	3.84
c_c^2	33.4	16.6	12.8	7.93	<u>0.56</u>

[a] χ_c^2: critical χ^2 according to Bartlett's test (eq 2.A2). χ_t^2: tabulated χ^2 (Fisher, 1970).

The optimization in the time domain favors an associative hydrogen adsorption equilibrium, which was found to be a simple linear function (eq 2.19). This is in line with Gut et al. (1979), who used similar rate equations. The denominator of their hydrogen adsorption equilibrium varied between:

$$1.14 < (1 + K_H P_{H_2}) < 1.23 \text{ for } 411 < T < 511 \text{ K}, 0.22 < P_{H_2} < 0.34 \text{ MPa} \qquad (2.21)$$

Therefore, their hydrogen function also showed an almost linear behavior.

First-order kinetics in hydrogen in liquid-phase hydrogenations are also reported for TAG hydrogenation and for Pt and Pd catalysts in FAME hydrogenation: Marangozis et al. (1977) concluded from a large set of experimental data of cottonseed and sesame seed hydrogenation over porous nickel, that hydrogen adsorption is first order for $P_{H_2} < 1.0$ MPa for monounsaturated TAG. Also for methyl oleate hydrogenation with Pt-on-carbon, Stenberg and Schöön (1985) found a linear

dependence on hydrogen pressure for 0.25 < P_{H_2} < 0.55 MPa and T = 433 K. Only Cordova and Hariott (1975) calculated for Pd-catalyzed methyl linoleate hydrogenation an order of 0.5 in hydrogen for the methyl oleate part, but they remarked that further data were needed to confirm the reaction order.

Associative hydrogen adsorption is, however, rather unexpected with regard to data from vapor-phase hydrogenations. Lidefelt et al. (1983) hydrogenated methyl oleate (0.015–0.11 kPa) on supported nickel catalyst at 421–487 K in excess of hydrogen (0.35–5.6 kPa) and nitrogen (to balance to 0.1 MPa total pressure). The observed order in hydrogen of 1.5 can be explained by dissociative hydrogen adsorption in competition with adsorption of oleate at the surface (Lidefelt et al., 1983). In the same equipment, Magnusson (1987a,b) found from H_2/D_2 exchange experiments that hydrogen adsorbs in a Rideal–Eley mechanism, which also assumes dissociation of the hydrogen molecules. But in the liquid phase, the $C_O/C_{H_2} \approx 1$ (gas phase: $C_O/C_{H_2} \approx 0.01$) which apparently changes the adsorption behavior of hydrogen from dissociative to associative.

A2B2-ass and A2B1-ass are indistinguishable according to Bartlett's test, but from a physical point of view, model A2B2 is preferred to A2B1, because A2B1 assumes both an adsorption step (B1) and an insertion of hydrogen into the double bond (A2) as rate-limiting steps. At the same time, the complementary reaction steps (A1 and B2) should proceed relatively quickly in the case of model A2B1, which is less likely than having two identical rate-determining steps such as in model A2B2.

From hydrogenation literature on rate-determining steps, the vast amount on ethylene hydrogenation should be mentioned. The HP mechanism has been proposed for these reactions as well (Horiuti and Polanyi, 1934). However, even for this relatively simple and widely investigated reaction, there still remains uncertainty on the rate-determining step (e.g., Prairie and Bailey, 1987). This shows how difficult the determination of rate-determining steps is.

Kinetic data on the migration of double bonds may give more insight in rate-determining steps. Van der Plank (1972b) studied migration effects of monoene FAME (liquid phase, $323 \leq T \leq 448$ K) and proved that if a FAME molecule enters the pores, in the absence of diffusion limitation, a migration reaction only occurs once before the FAME leaves the pores. Van der Plank and Van Oosten (1975) concluded from these data that the adsorption process must be relatively fast compared to the migration reaction and suggested that the rate-limiting step for the hydrogenation reaction should be the insertion of hydrogen into the half-hydrogenated intermediate

(the second hydrogen insertion, step C2). The migration studies thus showed a relatively fast adsorption process, which is supported by model A2B2, but from our analysis step C2 could not to be a rate-determining step.

2.4.3. Consequences of model A2B2. Model A2B2-ass can be used to investigate the hydrogenation rates of O and E, in relation to the isomerization rate, and their effect on the observed product distributions during the hydrogenation. Table 2.13 summarizes the parameters for model A2B2-ass. The confidence limits are calculated by use of the inverse Hessian matrix (Press et al., 1987), which only holds for one parameter fit (Emig and Hosten, 1974). Therefore, we have also applied the more generally applicable method of constant c^2-boundaries, as is described by Press et al. (1987). For our rate equations, both methods give almost the same results, where it should be remarked that the calculation of constant c^2-boundaries costs many more model evaluations (Emig and Hosten, 1974).

Table 2.13: Fitted Parameters Values for A2B2 (Associative Hydrogen Function) with 95% Confidence Limits

lumped parameters	reaction paths const.	fitted value	E_a[kJ/mol]
k_1	$k_{f,O}^{O,h} K_H$	4.14 ± 0.14 [a]	32.2 ± 0.7
k_2	$\bar{k}^{iso} K_H$	1.54 ± 0.15 [a]	47.2 ± 4.2
k_3	$k_{f,E}^{E,h} K_H$	3.94 ± 0.32 [a]	28.1 ± 3.1
k_4	K_S / K_M	0.32 ± 0.04 [b]	

[a] units: [kg$_l$/(kg$_{Ni}$ MPa s)]. [b] units: dimensionless.

Parameter k_1 and k_3 are almost equal, which means a comparable hydrogenation rate of O and E. With k_1 equal to k_3, the apparent rate equations of Gut et al. (1979) turn out to be similar to model A2B2-ass, so Gut et al (1979) implicitly assumed the first hydrogen insertion to be the rate-limiting step. Equal hydrogenation rate constants of O and E were also assumed by Grau et al. (1986, 1987b), in calculating global pseudo-first-order reaction constants. Their assumption of equal hydrogenation rates of O and E (k_1=k_3), based on the suggestion of Van der Plank and Van Oosten (1975), is justified by our study.

A constant ratio of the concentration of O (denoted by $C_{O,eq}$) and E ($C_{E,eq}$) and therefore constant conversion rates ($R_{O,eq}$ and $R_{E,eq}$, respectively) gives an observed equilibrium (K_{obs}) between O and E:

$$C_{E,eq} = K_{obs} C_{O,eq} \Rightarrow K_{obs} = \frac{R_{E,eq}}{R_{O,eq}} \tag{2.22}$$

However, this equilibrium observed during the hydrogenation is not necessarily the isomerization equilibrium, as can be illustrated by applying model A2B2:

$$\frac{R_E}{R_O} = \frac{-(k_3 + k_2)K_{obs} + k_2 K_{iso}}{-(k_1 + k_2 K_{iso}) + k_2 K_{obs}} = K_{obs} \tag{2.23}$$

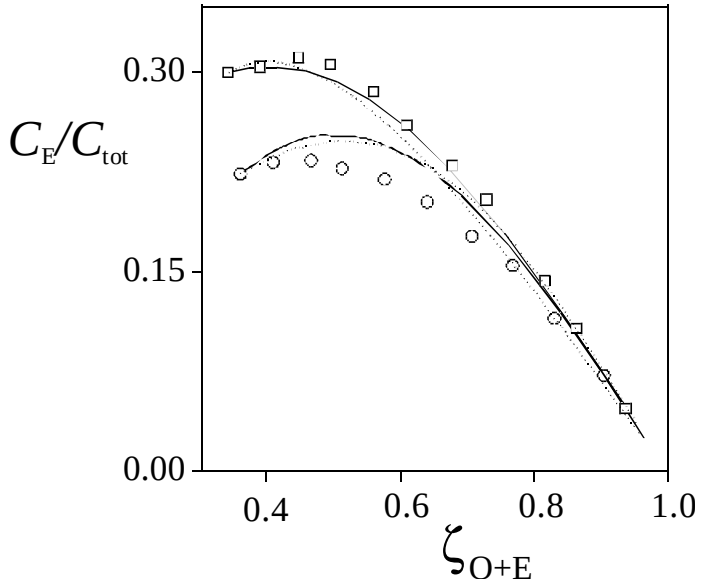

Figure 2.8. Experimental and simulated elaidate fractions for models A2B2 and A2B1 with associative hydrogen adsorption equilibrium versus conversion of double bonds for experiments at 0.50 and 0.08 MPa hydrogen pressure (393 K). Parameter values are in Table 2.13. ○, 0.50 MPa/393 K; □, 0.08 MPa/393 K; , simulated curve for A2B2; Λ, simulated curve for A2B1.

Only for $k_3 = k_1$, is $K_{obs} = K_{iso}$ obtained. From early kinetic data, $K_{iso} \approx 2.0$ (T = 393 K) was determined from an observed equilibrium between O and E during the reaction (Feuge et al., 1960; Litchfield et al., 1963; Stefanovic et al., 1978). This is rather low compared to independent measurements (K_{iso} = 3.6 at T = 393 K); Litchfield et al., 1963). Litchfield et al. (1963) noted an underestimation of the amount of *trans* in earlier literature data, due to inaccurate analysis. Another reason may be that the

calculated value of K_{obs} is influenced by kinetic rate constants. Therefore, an independent method is preferred for measuring the isomerization equilibrium, e.g., by using selenium, which isomerizes double bonds only, without any hydrogenation activity (Litchfield et al., 1963).

Model A2B2-ass shows some deviations in describing the isomerization reaction, which is expressed in Figure 2.8 in an overestimation of the E fraction in the 0.50 MPa experiment. This may arise from the formation of migration products at lower hydrogen pressures, but this has not been investigated. In our model evaluations, the kinetics of positional isomers are assumed to be the same, but especially at lower hydrogen pressures, the *trans* isomers of migration products are favored to *cis*, due to the formation of the π-allyl intermediate (Heertje et al., 1974; Van der Plank and van Oosten, 1975). The influence of diffusion limitation was checked by fitting the experimental data with the diffusion equations (eq 2.13) and using the rate expressions and optimised parameters of model A2B2 (see Table 2.13). In all experiments, the effectiveness factor proved to be close to 1 and the fit could not be improved, using the values of the diffusion coefficients mentioned in the introduction of this section.

The parameter values of model A2B2 (Table 2.13) can be compared to literature data of Gut et al. (1979): their value of k_2/k_1 = 0.33, is close to our value of 0.4. The ratio K_S/K_M = 0.32 is somewhat larger than 0.15 found by Gut et al. (1979). The adsorption of both saturated and unsaturated FAME on supported nickel surface is comparable, which indicates an interaction between methyl ester and the catalyst surface. The methyl ester may adsorb on acidic support sites, as was suggested by Rodrigo et al. (1992). The activation energy of the isomerization reaction, $E_{a,2}$ (47 kJ/mol) is 1.5 times larger than of the hydrogenation reactions ($E_{a,1}$ and $E_{a,3}$ are about 30 kJ/mol). Also Gut et al. (1979) found larger activation energies, being 33 kJ/mol for $E_{a,2}$, and a low 10 kJ/mol for $E_{a,1}$; the latter may be caused by diffusion limitation. Apart from Gut et al. (1979) only Hashimoto et al. (1971) used LHHW kinetics which can be compared to our data, but in a small temperature range (378–403 K). Hashimoto et al. (1971) calculated no influence of temperature.

Other literature values of activation energies for hydrogenation of monoene FAME and TAG using porous nickel catalysts are difficult to interpret because either a power law (Bern et al., 1975b; Susu et al., 1978) or first-order kinetics (Nielsen et al., 1960) were applied. Bern et al. (1975b) found an activation energy for the monoene hydrogenation of 75 kJ/mol, but calculated a reaction order in hydrogen varying from 0.24 at 413 K to 0.54 at 473 K (first order in rapeseed oil). This low reaction order

strongly influences the calculated value of the activation energy. Also the activation energy of Susu et al. (1978), 17.7 kJ/mol is strongly influenced by (extremely) high reaction orders in hydrogen (7.1) for the hydrogenation reaction. The activation energy of 40 kJ/mol calculated by Nielsen et al. (1960) for first-order kinetics in FAME is comparable to ours (30 kJ/mol), particularly because the reaction order for model A2B2-ass becomes first order at higher conversion.

2.5. Conclusions

Kinetic expressions for the hydrogenation reaction rates of methyl oleate and elaidate were derived on the basis of the Horiuti–Polanyi mechanism. Kinetic experiments in absence of diffusion limitation were carried out for $333 \leq T £ 443$ K, $0.02 \leq P_{H_2} £ 0.50$ MPa and various compositions of oleate, elaidate and stearate.

The experiments were fitted in both the conversion and time domain. The model with a rate limitation in the first hydrogen insertion in the double bonds of adsorbed oleate and elaidate proved to be the most likely. Activation energies of 30 kJ/mol for the hydrogenation reactions of oleate and elaidate and 44 kJ/mol for the isomerization reaction were found. Further, it is shown that the isomerization constant preferably must be obtained from independent isomerization experiments rather than from fitting hydrogenation data in kinetic models.

Appendix: Model Selection

The statistically most significant model was selected after a multistep optimization of the (compound) model parameters on the basis of all experimental curves simultaneously. The Levenberg–Marquardt algorithm (Press et al., 1987) optimized the parameters for the minimal c^2, defined as the deviation between experimental and model fractions for $N_{e,d}$ experimental points of the N_e hydrogenation runs with $N_{e,i}$ components:

$$c^2 = \frac{1}{N_e} \sum_{e=1}^{N_e} \frac{1}{N_{e,d} N_{e,i}} \sum_{i=1}^{N_{e,i}} \sum_{d=1}^{N_{e,d}} \frac{(C^e_{e,i,d} - C^m_{e,i,d})^2}{s^2_{i,d}} \qquad (2.A1)$$

Here, $C^e_{e,i,d}$ and $C^m_{e,i,d}$ are the experimentally observed and the calculated model concentration values for the *e*th experiment, *i*th component of the *d*th data point, respectively, and $s_{i,d}^2$ is the corresponding experimental variance for the *i*th component and *d*th data point. The c^2 values of all models were compared in order to select the most likely model. Here we used Bartlett's test to test whether differences in accuracy of the various models were statistically significant (Dumez et al., 1977; Graaf et al., 1988a,b).

For a selected set of *H* models, the Bartlett test calculates the critical c_c^2:

$$c_c^2 = \frac{\ln S^2_{av} \sum_{h=1}^{H} df_h - \sum_{h=1}^{H} df_h \ln S^2_h}{1 + \frac{1}{3(H-1)} \left(\sum_{h=1}^{H} df_h^{-1} - \left(\sum_{h=1}^{H} df_h \right)^{-1} \right)} \qquad (2.A2)$$

with S_h^2 the total variance between the experimental series and model *h* and S_{av}^2 the average total variance of *H* models (Dumez et al., 1977):

$$S^2_h = df_h^{-1} \sum_{e=1}^{N_e} \sum_{i=1}^{N_{e,i}} \sum_{d=1}^{N_{e,d}} (C^e_{e,i,d} - C^m_{e,i,d})^2 \qquad (2.A3)$$

$$S_{\mathrm{av}}^2 = \frac{\sum_{h=1}^{H} \mathrm{df}_h S_{\mathrm{h}}^2}{\sum_{h=1}^{H} \mathrm{df}_h} \qquad (2.A4)$$

df_h represents the degrees of freedom for the fit of the hth model to the experimental series and is calculated by

$$\mathrm{df}_h = \sum_{e=1}^{N_{\mathrm{e}}} [(N_{e,d} - 1) N_{e,i}] - N_{h,\mathrm{fit}} \qquad (2.A5)$$

$N_{h,\mathrm{fit}}$ is the number of estimated parameters of the hth model. Whenever c_{c}^2 exceeds the tabulated value $c_{\mathrm{t}}^2(H - 1)$ (Fisher, 1970), the model giving rise to the largest S_h^2 was discarded and c_{c}^2 remained below the tabulated value.

For the calculation of the degrees of freedom, each experimental line of a batch run is treated as one experimental data point ($N_{e,d}$). The approach of taking only 1 degree of freedom for an experimental line is most conservative and minimizes the influence of unpredictable exerimental errors as slight (initial) temperature variations and nonuniformity's catalyst activity. Both the model evaluation and the 95% confidence limits are determined with this conservative number of degrees of freedom.